# Validation of the vertical profiles of HCl over the wide range of the stratosphere to the lower thermosphere measured by SMILES

Seidai Nara[1,2], Tomohiro O. Sato[1], Takayoshi Yamada[1], Tamaki Fujinawa[3], Kota Kuribayashi[4], Takeshi Manabe[5], Lucien Froidevaux[6], Nathaniel J. Livesey[6], Kaley A. Walker[7], Jian Xu[8], Franz Schreier[8], Yvan J. Orsolini[9], Varavut Limpasuvan[10], Nario Kuno[2], and Yasuko Kasai[1,2]

[1]National Institute of Information and Communications Technology, Nukui-kita, Koganei, Tokyo 184-8795, Japan
[2]University of Tsukuba, Tennodai, Tsukuba, Ibaraki 305-8577, Japan
[3]National Institute of Environmental Studies, Onogawa, Tsukuba, Ibaraki 305-8506 Japan
[4]Mynavi Corporation, Tokyo, Japan
[5]Osaka Prefecture University, Gakuen-cho, Naka-ku, Sakai, Osaka 599-8531, Japan
[6]Jet Propulsion Laboratory, California Institute of Technology, Pasadena, CA USA
[7]Department of Physics, University of Toronto, 60 St. George Street, Toronto, Ontario, M5S 1A7, Canada
[8]German Aerospace Center (DLR), Remote Sensing Technology Institute, 82234 Oberpfaffenhofen, Germany
[9]Norwegian Institute for Air Research (NILU),Kjeller, Norway
[10]School of Coastal and Marine Systems Science, Coastal Carolina University, Conway, South Carolina, USA

**Correspondence:** Y. Kasai (ykasai@nict.go.jp)

**Abstract.** Hydrogen chloride (HCl) is the most abundant (more than 95 %) among inorganic chlorine compounds $Cl_y$ in the stratosphere. The HCl molecule has been observed to obtain long-term quantitative estimations of total budget of the stratospheric anthropogenic chlorine compounds. In this study, we provided HCl vertical profiles at altitudes of 16–100 km using the superconducting submillimeter-wave limb-emission sounder (SMILES) from space. We used the SMILES Level-2

5   research product version 3.0.0. The period of the SMILES HCl observation was from October 12, 2009 to April 21, 2010, and the latitude coverage was 40°S–65°N. The average HCl vertical profile showed an increase with altitude up to the stratopause (∼45 km), approximately constant values between the stratopause and the upper mesosphere (∼80 km), and a decrease from the mesopause to the lower thermosphere (∼100 km). This behavior was observed in the all latitude regions, and reproduced by the SD-WACCM model. We compared the SMILES HCl vertical profiles in the stratosphere and lower mesosphere with

10   HCl profiles from MLS on the Aura satellite, as well as from ACE-FTS on SCISAT and from TELIS (balloon-borne). The TELIS observations were performed using the superconductive limb emission technique, as used by SMILES. The globally averaged vertical HCl profiles of SMILES well agreed with those of MLS and ACE-FTS within 0.25 and 0.2 ppbv between 20 and 40 km, respectively. The SMILES HCl concentration was smaller than those of MLS and ACE/FTS as the altitude increased from 40 km, and the difference was approximately 0.4–0.5 ppbv at 50–60 km. The difference between SMILES and

15   TELIS HCl observations was about 0.3 ppbv in the polar winter region between 20 and 34 km, except near 26 km. SMILES HCl error sources that may cause discrepancies with the other observations are investigated by a theoretical error analysis. We calculated errors caused by the uncertainties of spectroscopic parameters, instrument functions, and atmospheric temperature profiles. The jacobian for the temperature explains the negative bias of the SMILES HCl concentration at 50–60 km. The HCl

vertical profile from the upper troposphere to the lower thermosphere is reported for the first time from SMILES observations;
20  the data quality is quantified by comparisons with other measurements and via theoretical error analysis.

## 1  Introduction

Hydrogen chloride (HCl) is the most abundant species of all total inorganic chlorine compounds $Cl_y$ in the stratosphere.
More than 95 % of $Cl_y$ exists as HCl at about 1 hPa (∼50 km) (see Froidevaux et al. (2008)). Thus, HCl has been used for
long-term quantitative estimates of the total budget of stratospheric chlorine (WMO, 2010). Stratospheric HCl vertical profiles
25  have been observed globally by several satellites. The halogen occultation experiment (HALOE) on the Upper Atmosphere
Research Satellite measured the stratospheric HCl profiles continuously from late 1991 through November 2005 (Russell et al.,
1996). Comparisons of HCl profiles obtained by the Aura Microwave Limb Sounder (MLS) and the Atmospheric-Chemistry-
Experiment Fourier-Transform Spectrometer (ACE-FTS) have been reported by Froidevaux et al. (2008) and Mahieu et al.
(2008). These profiles agreed within 5% (0.15 ppbv) at 0.5 hPa (∼53 km). The Aura/MLS and ACE-FTS HCl concentrations
30  were larger (by 10% – 20%) than those from HALOE HCl (WMO, 2010). Balloon-borne remote sensing in polar winter region
was performed using the TErahertz and submillimeter LImb Sounder (TELIS) from 2009 to 2011 (Birk et al., 2010). Xu et al.
(2018) reported the error analysis and comparison of some trace gas profiles provided by TELIS.

The superconducting submillimeter-wave limb-emission sounder (SMILES) was launched in 2009 to observe the atmo-
spheric compositions of ozone and species related to the stratospheric ozone destruction cycle including HCl (Kikuchi et al.,
35  2010). The SMILES mission is a joint project of the Japan Aerospace Exploration Agency and the National Institute of Infor-
mation and Communications Technology (NICT). The SMILES is an instrument used to conduct limb observations from the
International Space Station (ISS) using super-sensitive 4 K superconducting receivers in the submillimeter-wave regions (625
and 649 GHz bands). The non-sun-synchronous circular orbit of the ISS gave us an opportunity for observations of HCl pro-
files at different local times. The unprecedented low noise of the SMILES instrument provided a sensitivity 10 times superior
40  to those of previous microwave/sub-millimeter limb emission instruments used to observe HCl spectra from space (Kikuchi
et al., 2010). The SMILES observations were used to reveal small abundances of atmospheric species in the stratosphere and
mesosphere (e.g. Sato et al. (2017); Yamada et al. (2020))

A comparison of the HCl profiles inside the Antarctic vortex has been performed for November 19—24, 2009 using the
SMILES, Aura/MLS, and ACE-FTS data (Sugita et al., 2013). The SMILES HCl values (version 2.1.5 of NICT products)
45  agreed within 10 % (0.3 ppbv) with those of the MLS and ACE-FTS HCl data between the potential-temperature levels of 450
and 575 K and 425 and 575 K, respectively. The HCl climatology using SMILES NICT version 2.1.5 was reported by Kreyling
et al. (2013).

In this study, SMILES observations of HCl vertical profiles from 16–100 km, including the upper mesosphere and lower
thermosphere (MLT) region. We used the SMILES NICT Level-2 product version 3.0.0 (v300), which was released in late 2012
50  (http://smiles.nict.go.jp/pub/data/index.html). HCl vertical profiles from the upper troposphere to the lower thermosphere are
reported for the first time. We perform a validation of the SMILES HCl vertical profiles by comparisons with the corresponding

**Table 1.** SMILES specification

| Parameter | Characteristics |
| --- | --- |
| Orbit | Non-sun-synchronous orbit |
| | Inclination angle $51.6°$ |
| | Altitude 340–360 km |
| | $\sim$ 90-min orbital period |
| Latitude coverage | $38°$S-$65°$N(nominal) |
| Measurement geometry | Limb scan |
| Number of scans | 1630 scans per day |
| Integration time | 0.47 s |
| Frequency range | 624.32–625.52 GHz (Band-A) |
| | 625.12–626.32 GHz (Band-B) |
| | 649.12–650.32 GHz (Band-C) |
| Receiver system | SIS[*1] mixer and HEMT[*2] amplifiers |
| Spectrometer | Acousto-Optical Spectrometers |
| | (AOS1 and AOS2) |
| Frequency resolution | 0.8 MHz |
| System noise temperature | $\sim$ 350 K |

*1: Superconductor-Insulator-Superconductor, *2: High-Electron-Mobility Transistor

global model results of SD-WACCM, satellite observations from MLS and ACE-FTS, balloon-borne observations from TELIS and we provide a SMILES HCl error analysis.

The SMILES HCl observations and retrieval procedure are described in Sect. 2. The HCl vertical profile derived by the
55  SMILES product and comparisons of HCl distribution between $40°$S–$60°$N with SD-WACCM are shown in Sect. 3. Results of HCl comparisons between SMILES and other instruments are described in Sect. 4. An estimation of the systematic and random errors is presented in Sect. 5. Section 6 describes our conclusions.

## 2   SMILES HCl observation

The SMILES instrument had been attached to the Japanese Experimental Module (JEM) on the ISS, since September 2009.
60  The period of the SMILES observation was from October 12, 2009 to April 21, 2010. The ISS has a non-sun-synchronous circular orbit with an inclination angle of $51.6°$ with respect to the equator. The height of the ISS changed slowly over the observational period ranging 340–360 km. We tilted the line-of-sight at a $45°$ angle in the direction of the forward movement of the ISS to observe the northern polar region. The SMILES parameters are summarized in Table 1. The details of the SMILES observation are described in Kikuchi et al. (2010) and in an ozone-validation paper Kasai et al. (2013), respectively.

65    Herein, we briefly describe the SMILES atmospheric observations in terms of the HCl spectra. The SMILES had three
frequency bands in the submillimeter-wave regions, Band A (624.32–625.52 GHz), Band B (625.12–626.32 GHz), and Band
C (649.12–650.32 GHz). Each single-scan provided a combination of two out of three of the frequency bands: Bands A+B,
C+B, and C+A. The combinations changed on a daily basis, as described in Kikuchi et al. (2010). The rotational transitions
of two HCl isotopologues were located in Bands B and A for $H^{35}Cl$ at 625.9 GHz and $H^{37}Cl$ at 624.9 GHz, respectively. Two
70    acousto-optical spectrometers (AOSs) were equipped in the SMILES instrument. The spectral resolution obtained by AOS1
and AOS2 was 0.8 MHz. The band configuration for each HCl isopologues had three patterns as follows:,

a) $H^{37}Cl$ observation by Band-A with AOS1,

b) $H^{37}Cl$ observation by Band-A with AOS2,

c) $H^{35}Cl$ observation by Band-B with AOS2.

75    Band-B was always associated with AOS2.

Figure 1 shows the number of observations obtained for $H^{35}Cl$ (Band-B) and $H^{37}Cl$ (Band-A) for $5°$ latitude bins during
the SMILES observational period. It should be noted that the sampling is not homogeneously distributed for the SMILES
observations. The SMILES instrument was sometimes not in operation, for example, when the ISS was boosted up from a
low to a high altitude, and the solar panels disturbed the observational line-of-sight. The SMILES observational latitude range
80    was $65°N–38°S$ in nominal operations, and changed to $38°N–65°S$ when the ISS performed a yaw maneuver of $180°$, which
happened three times during the 7-month-long observational period.

We used the SMILES NICT Level 2 product version 3.0.0 (v300) for this study. The general method of v300 for the HCl
retrieval is similar to that of the Level 2 product version 2.1.5 (v215) (Kasai et al., 2013). The major updates from the v215
product are as follows: 1) An improvement in the spectrum calibration, particularly for the gain non-linearity of the receiver
85    system (Ochiai et al., 2013), 2) An improvement in the accuracy of the tangent height estimation (Ochiai et al., 2013), and
3) An update of the temperature retrieval. The level 1b spectrum data version 008 was used for the SMILES NICT Level 2
product v300 (Ochiai et al., 2013). The spectroscopic parameters for the HCl retrieval were based on Cazzoli and Puzzarini
(2004) and Laboratory measurement, as summarized in Table.2. We used only the $H^{35}Cl$ data because the intensities of the
$H^{37}Cl$ spectra were weaker than those of $H^{35}Cl$, as shown in Fig. 2.
90    The criteria for the selection of the $H^{35}Cl$ profiles used in this study are as follows: (1) $\chi^2$ less than 0.8. $\chi^2$ is defined by

$$\chi^2 = [\mathbf{y} - \mathbf{F}(\mathbf{x})]^{\mathbf{T}}\mathbf{S}_\epsilon^{-1}[\mathbf{y} - \mathbf{F}(\mathbf{x})] + [\mathbf{x} - \mathbf{x}_a]^{\mathbf{T}}\mathbf{S}_a^{-1}[\mathbf{x} - \mathbf{x}_a] \qquad (1)$$

$\mathbf{y}$ is observed spectrum, $\mathbf{S}_\epsilon$ is the covariance matrix of the measurement noise, $\mathbf{x}_a$ is the a priori state, $\mathbf{S_a}$ is the covariance
matrix of $\mathbf{x}_a$, and $\mathbf{F}(\mathbf{x})$ is the forward model depending on the state vector $\mathbf{x}$. The forward model is essentially the atmospheric
radiative transfer and the instrument model. (2) measurement response, MR, between 0.8 and 1.2 for each vertical grid. MR is
95    defined by

$$\mathrm{MR}[i] = \sum_j \mathbf{A}[i, j] \qquad (2)$$
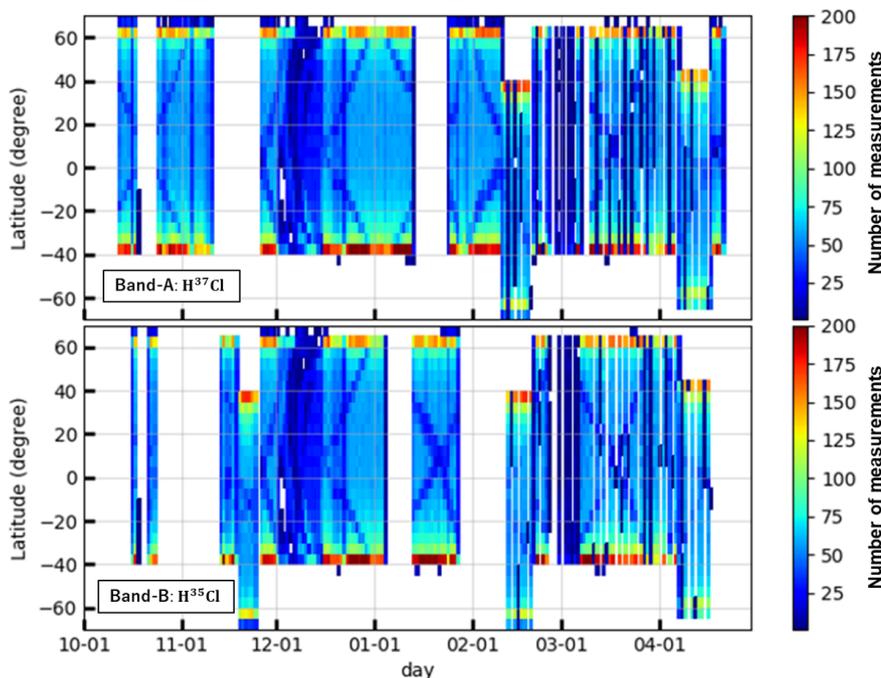
**Figure 1.** Number of HCl observations for a $5°$ latitude bin in 1 day for the range of SMILES observational latitudes and period (October 12, 2009 – April 21, 2010). The top and bottom panels show the number of observations from Band-A ($H^{37}Cl$) and Band-B ($H^{35}Cl$), respectively.

**Table 2.** Spectroscopic line parameters measured in the laboratory and used in the processing.

| Species | Line frequency [MHz] | Air-broadening [MHz/Torr] /temperature dependence | Frequency shift [MHz] |
|---|---|---|---|
| $H^{35}Cl$ | 625 901.6627[a] <br> 625 918.7020[a] <br> 625 931.9977[a] | 3.39/0.72[b] | 0.145[b] |
| $H^{37}Cl$ | 624 964.3718[a] <br> 624 977.8059[a] <br> 624 988.2727[a] | 3.39/0.72[b] | 0.145[b] |

a: Laboratory measurements by Cazzoli and Puzzarini (2004). b:Baron et al. (2011)

**A** is the averaging kernel matrix. A value of MR near unity indicates that most of the information in the retrieval results is provided by observations. A low value of MR indicates that the retrieval results are largely influenced by the a priori state and are forced to be identical to a priori values.

100     An example $H^{35}Cl$ profile and its averaging kernel are presented in Fig. 3 for the single scan spectrum observation at latitude of $38.3°$ N, longitude of $12.7°$E, and solar zenith angle (SZA) of $160.9°$ on 15 November 2009. We assumed that the natural
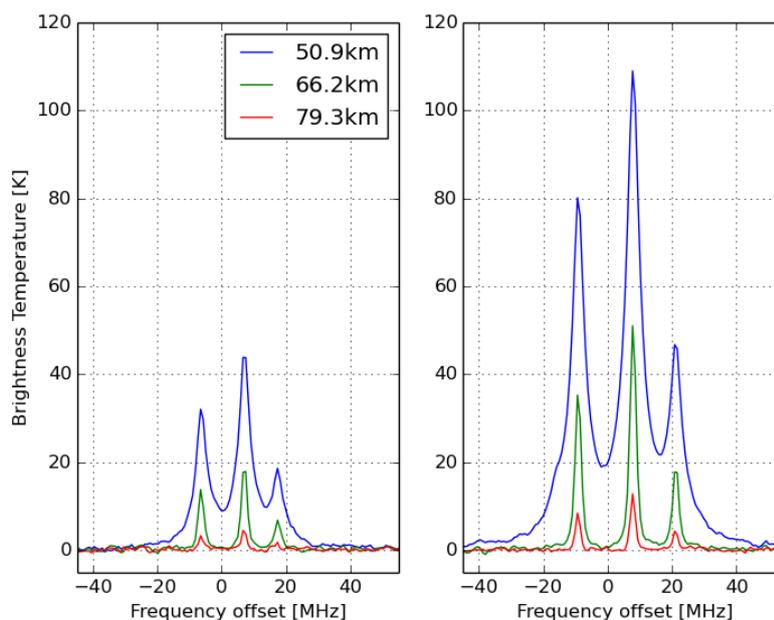
**Figure 2.** Left: An example of the H$^{37}$Cl spectrum observed by SMILES from a single scan measurement. Tangent heights are approximately 50, 65, and 80 km. Center frequency is 624.98 GHz. Right: An example of the H$^{35}$Cl spectrum for the same condition as for the H$^{37}$Cl spectrum. Center frequency is 625.92 GHz.

isotopic abundance of H$^{35}$Cl/HCl was 0.7576 for these retrievals. The peak values of the averaging kernels for the SMILES H$^{35}$Cl profiles exceeded 0.8 in the height range of 16 km to 90 km ($\sim$ 100 hPa to 0.001 hPa) as shown in Fig. 3. The full width at half maximum (FWHM) of the averaging kernels is approximately 3 –4 km at altitudes of 18 km–50 km and becomes
105 greater than 5 km for the altitude of 50 km–90 km.

## 3 Vertical and latitudinal distribution of SMILES HCl

In this section, we provide the HCl vertical profiles derived from the SMILES NICT Level 2 product v300. Figure 4 (A) shows the HCl zonal mean distribution in the latitudinal range from 40°S to 60°N. The observation periods are October 16, 2009–December 15, 2009 (Left), December 16, 2009–February 15, 2010 (Middle), and February 16, 2010–April 17, 2010
110 (Right). The HCl vertical profile showed an increasing with the altitude increased below the stratopause ($\sim$45 km), approximately constant between the stratopause and the upper mesosphere ($\sim$80 km), and decreased with the altitude increasing from the mesopause to the lower thermosphere ($\sim$100 km). This behavior was reproduced by the Whole Atmosphere Community Climate Model version 4 (WACCM4) in specified dynamics configuration (SD-WACCM) (Lamarque et al., 2012; Limpasuvan et al., 2016), see the panel (B). Differences of HCl abundance between SMILES and SD-WACCM are shown in the panel
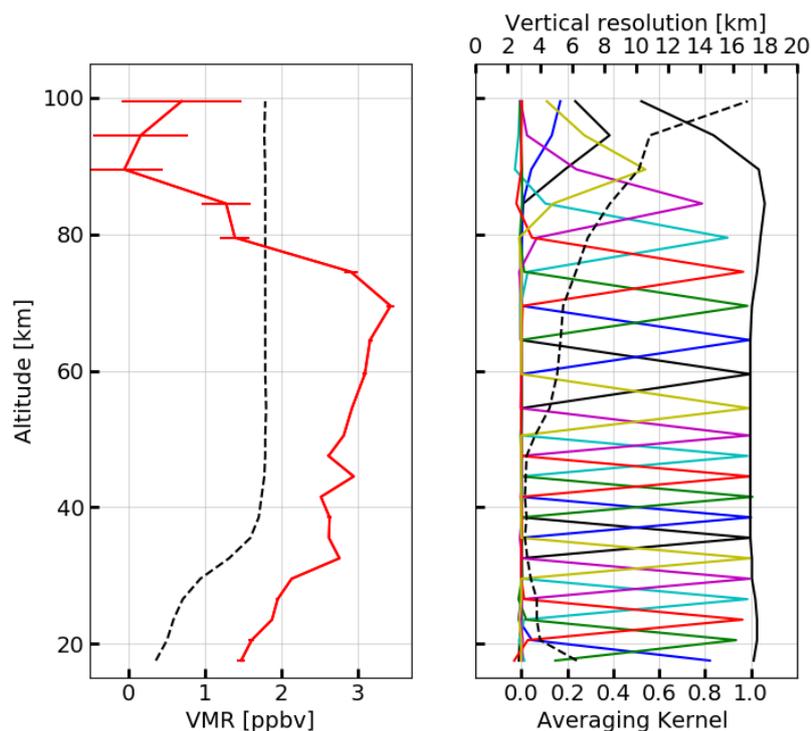
**Figure 3.** Left: An example of a HCl profile retrieved from the H$^{35}$Cl spectrum on November 15, 2009 at a latitude of 38.3°N, longitude 12.7°E, and SZA of 160.9°. The solid red line indicates the retrieved HCl volume mixing ratio (VMR), and the error bar is the root sum square of the smoothing and measurement errors. The dashed black line is an a priori HCl profile used for the retrieval procedure. The right panel shows the averaging kernel,the measurement response (indicated by the thick black line) and the FWHM of the averaging kernel profile (indicated by the thick dashed black line).

115  (C). The SMILES HCl abundance agrees well with SD-WACCM simulation (within 0.1 ppbv) in the stratosphere and middle mesosphere. At 70 − 100km, the SMILES HCl abundances are about 0.4 − 1.3 ppbv larger than in the SD-WACCM simulation. For these comparisons, the SD-WACCM profiles are interpolated linearly for each SMILES observation point and time from the nearest model positions and times. In the specified dynamics configuration, the simulated meteorological fields in the troposphere and stratosphere are constrained to the Global Modeling and Assimilation Office Modern-Era Retrospective Analysis

120  for Research and Applications (Rienecker et al., 2011). The horizontal resolution of SD-WACCM simulation is 1.9° and 2.5° for latitude and longitude, respectively. The vertical grid is from the ground to 150 km with 88 levels, and the time resolution is 3 hours. The panel (D) shows the number of selected SMILES observation.
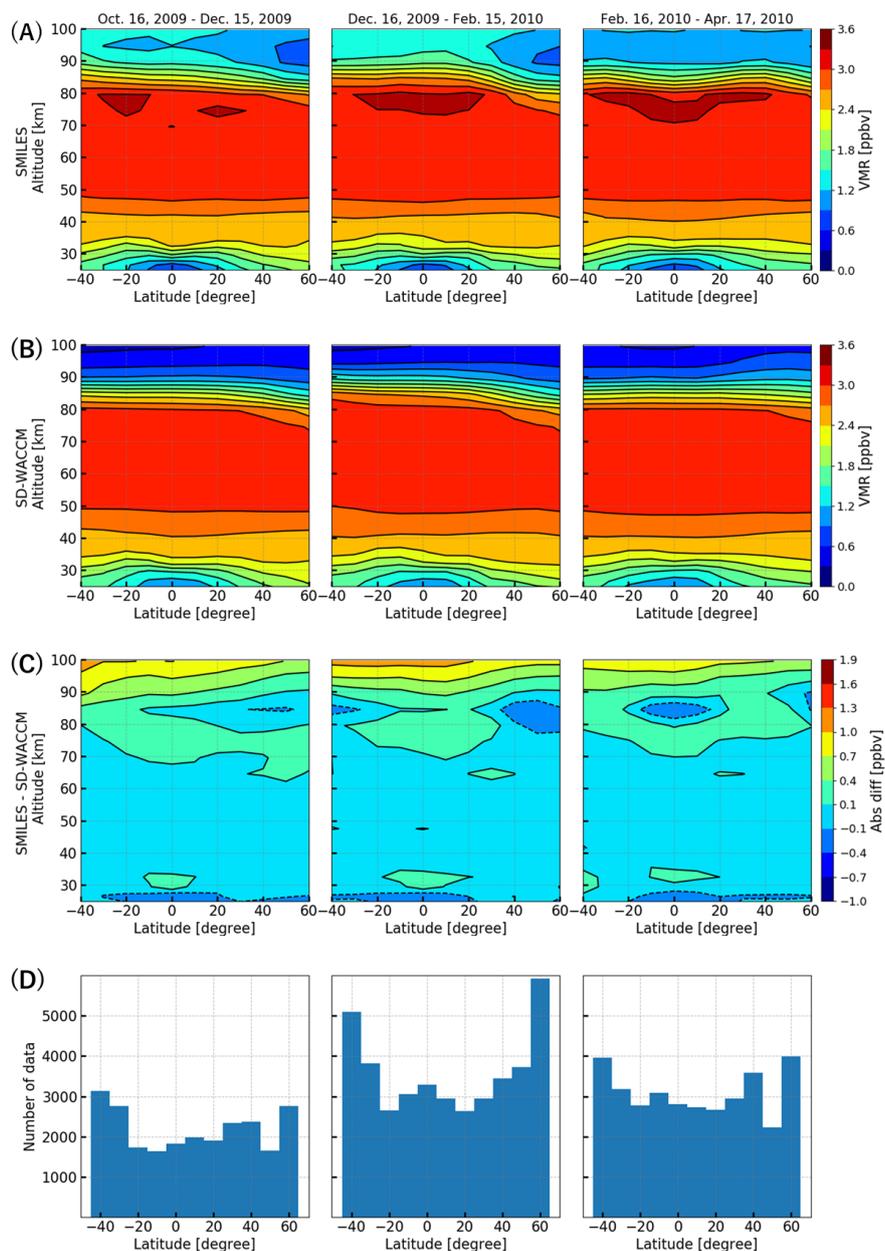
**Figure 4.** Zonal mean distribution of HCl from SMILES, SD-WACCM and their differences (SMILES - SD-WACCM) are shown in rows (A), (B), and (C), respectively. Each panel displays distributions as a function of latitude (x-axis) and altitude (y-axis) in three time range. The latitude range covers between 40°S and 60°N. The number of HCl profiles observed by SMILES is described in (D) row as a histogram versus latitude. Left panel: Time range between October 16, 2009 and December 15, 2009. Middle panel: Between December 16, 2009 and February 15, 2010. Right panel: Between February 16, 2010 and April 17, 2010. The data was averaged within a latitude bin of 10°.

# 4 Comparison of SMILES HCl profile with those obtained using other instruments

We performed a comparison between SMILES HCl products and other datasets obtained using the MLS on the Aura satellite,

125 the ACE-FTS on the SCISAT satellite, and the balloon-borne TELIS instrument. The characteristic of instruments and datasets are summarized in Table 3. The mean absolute difference between SMILES and the other instrument is defined as

$$\Delta_{\mathrm{abs}}(z) = \frac{1}{N(z)} \sum_{i=1}^{N(z)} x_c(z) - x_s(z), \tag{3}$$

where $x_s(z)$ and $x_c(z)$ are the HCl volume mixing ratio (VMR) at an altitude $z$ for SMILES and the other instrument, respectively. The mean relative difference (in percentage) is given by

130 $$\Delta_{\mathrm{rel}}(z) = \frac{1}{N(z)} \sum_{i=1}^{N(z)} \frac{x_c(z) - x_s(z)}{(x_c(z) + x_s(z))/2} \times 100. \tag{4}$$

The coincidence criteria between the SMILES observations and those of the other instruments was set to within $2°$ for latitude, $8°$ for longitude, and $5\,\mathrm{h}$ for time, following the previous work of the MLS observations (Froidevaux et al., 2008).

**Table 3.** Characteristics of instruments and data sets used in the comparison.

| Instrument &Platform | Measurement type - | Time period overlapped with SMILES (yyyy/mm/dd) | Data version | Number of coincident observations |
|---|---|---|---|---|
| MLS Aura | Limb emission sub-mm/microwave | 2010/01/24 - 2010/01/27 (Band-13) | 4.2 | 4356 |
| ACE-FTS SCISAT | Solar occultation mid IR | 2009/10/16 - 2010/04/17 | 4.0 | 935 |
| TELIS Balloon borne | Limb emission submm/THz | 2010/01/24 | 3v02 | 4 |

## 4.1 Comparison with Aura/MLS

The Aura satellite has a sun-synchronous orbit with an ascending node at 1:45 PM local time (Waters et al., 2006). The

135 measurements cover latitudes from $82°$S to $82°$N and provide approximately 3500 vertical profiles each day. We used version 4.2 of the Aura/MLS HCl profiles for these comparisons. The Aura/MLS team provided two HCl products one from spectral band 13 (HCl-640-B13) and one from band 14 (HCl-640-B14). The HCl-640-B13 product is available for the pressure region between $100\,\mathrm{hPa}$ and $0.32\,\mathrm{hPa}$. The single profile precision of HCl-640-B13 is less than $0.8\,\mathrm{ppbv}$ ($25\%$) in the stratosphere, and the estimated accuracy is approximately $0.3\,\mathrm{ppbv}$ ($10\%$) (Livesey et al., 2018). The vertical and horizontal resolutions

140 are 3–5 km and 200–400 km, respectively. We used the recommended parameters "Status," "Quality," and "Convergence" for screening the Aura/MLS data based on Livesey et al. (2018). The good profiles were selected using (1) Quality $< 1.2$, (2)

Convergence $> 1.05$, and (3) Status $=$ Even. The SMILES profiles were linearly interpolated onto the MLS pressure grid for the comparisons.

Figure 5 shows a comparison of the HCl vertical profiles derived from SMILES and Aura/MLS in the SMILES latitude
145 range. The total number of coincident profile pairs was 4356. The HCl profiles from the SMILES measurements agreed with those of MLS within 0.25 ppbv between 20 and 40 km (50–3 hPa), while large biases about 0.4 ppbv were confirmed between 40 and 55 km (3–0.32 hPa). The differences between HCl profiles increases from the stratosphere to the mesosphere. Figure 6 shows the zonal mean absolute differences averaged for $5°$ latitude bins. The differences did not change with latitude in the altitude region between 35–55 km (7–0.32 hPa).

150 Figure 7 displays more detailed features of the differences between the SMILES and MLS profiles. Panels (A) of Fig. 7 show the averaged HCl vertical profiles of SMILES (blue) and MLS (red), and the absolute difference in each latitude region ($40°$S–$20°$S, $20°$S–$20°$N, $20°$N–$50°$N, and $50°$N–$65°$N). Panels (B) show the latitudinal distribution averaged in $5°$ bins for SMILES (blue) and MLS (red) at 30, 40, and 50 km. The error bar shows the $1\ \sigma$ variability for each latitude grid. In the equatorial regions, the SMILES HCl profiles were 0.5 ppbv larger than those of MLS at below 30 km (10 hPa) . There is a
155 possibility that this difference was caused by water vapor. The SMILES HCl profile was retrieved without considering water vapor effect and the influence of the water vapor was thus one of the possible results of the latitudinal difference. On the other hand, the HCl profiles from the SMILES measurements were 0.4 ppbv less than those of MLS in all latitude regions at 50 km.

### 4.2 Comparison with SCISAT/ACE-FTS

The ACE-FTS is an instrument mounted on the Canadian SCISAT satellite. SCISAT moves along an orbit at a 650 km alti-
160 tude and is inclined at $74°$ to the equator (Bernath et al., 2005). The ACE comprises two instruments: the Fourier Transform Spectrometer (ACE-FTS) and the Measurement of Aerosol Extinction in the Stratosphere and Troposphere Retrieved by Occul- tation (ACE-MAESTRO). The HCl observation has been performed using ACE-FTS. The ACE-FTS observes solar occultation spectra in the infrared spectral region ($750-4400\ \mathrm{cm}^{-1}$) with a high spectral resolution ($0.02\ \mathrm{cm}^{-1}$). We used ACE-FTS HCl profiles from the version 4.0 software, which is the latest data version.The vertical resolution of the ACE-FTS HCl retrieval
165 is 3–4 km, and the values from the retrieval grid are interpolated onto the 1-km grid, using a piecewise quadratic method (Bernath et al., 2005). In this study, we used the data within $\pm3$-MAD from the median to remove significantly large positive and negative biases based on Boone et al. (2019).

Figure 8 presents the comparison of the HCl vertical profiles between SMILES and ACE-FTS in the latitude range of $40°$S– $65°$N. The total coincident data number was 945. The SMILES HCl profiles agreed with those of the ACE-FTS by 0.2 ppbv
170 between 20 and 40 km (50–2 hPa), while 0.5 ppbv (15%) less than those of ACE-FTS above 40 km. This negative bias in the SMILES HCl concentration was confirmed as in the case of the MLS–SMILES comparison. The results of the comparison with the ACE-FTS for each latitudinal region are presented in Fig. 9 (A) in a manner similar to Fig. 7 (A). In the tropic region, a large discrepancy was observed at an altitude altitude of 25 km because of relativity poor sampling number. The HCl profiles observed using the SMILES were about 0.5 ppbv (15%) less than those of ACE-FTS for each latitudinal region above 50 km.
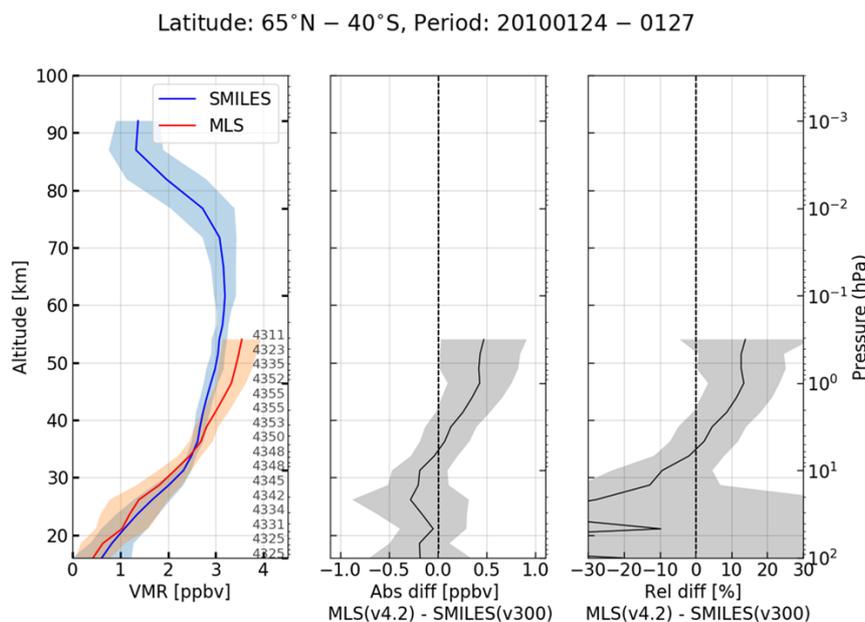
**Figure 5.** Comparison between SMILES and MLS profiles from January 24, 2010 to January 27, 2010. Left: mean HCl VMR values (solid lines) and $1\,\sigma$ (shaded areas) for SMILES and MLS. The blue and red lines indicate the SMILES HCl profiles and MLS profiles, respectively. Middle: The absolute difference between the SMILES and MLS profiles calculated using Eq (3). Right: The relative difference between the SMILES and MLS profiles calculated using Eq (4).

The period of the SMILES H$^{35}$Cl observation (from Oct 16, 2009 to Apr 17, 2010) was covered by the ACE-FTS observation period, while the MLS Band-13 observation period had an overlapped of only 4 days. We analyzed the difference between SMILES and ACE-FTS for each month and conformed the seasonal variation of the bias. Figure 9 (B) shows a seasonal variation of the difference between the SMILES and ACE-FTS profiles in the northern hemisphere (from 30°N–65°N latitude range). The upper panels in Fig. 9 (B) show a mean of the SMILES (blue) and ACE-FTS (red) profiles for each month at three altitude levels. The difference for every month, shown in the lower panels, was represented by the mean for each month at each altitude, and the error-bar showed the $1\,\sigma$ standard deviation. No significant seasonal dependence of the difference was observed. The difference of HCl value from these measurements was consequently about 0.5 ppbv at 50 km.

### 4.3 Comparison with balloon-borne instrument TELIS

The TELIS (Birk et al., 2010) is a balloon-borne THz/sub-millimeter-wave spectrometer with superconductive 4K technology similar to that of SMILES. TELIS was one of the instruments used in the balloon observation campaigns for three winters (2009–2011) in Kiruna, Sweden. Limb observations were performed from a flight altitude of 30–35 km, toward the stratosphere and the upper troposphere with 1.5–2 km vertical sampling. TELIS was used to observe H$^{37}$Cl at the transition frequency of 1873.4 GHz in the 1.8 THz channel (Level-1b version 3v02), which corrected non-linearity problems in the radiometric
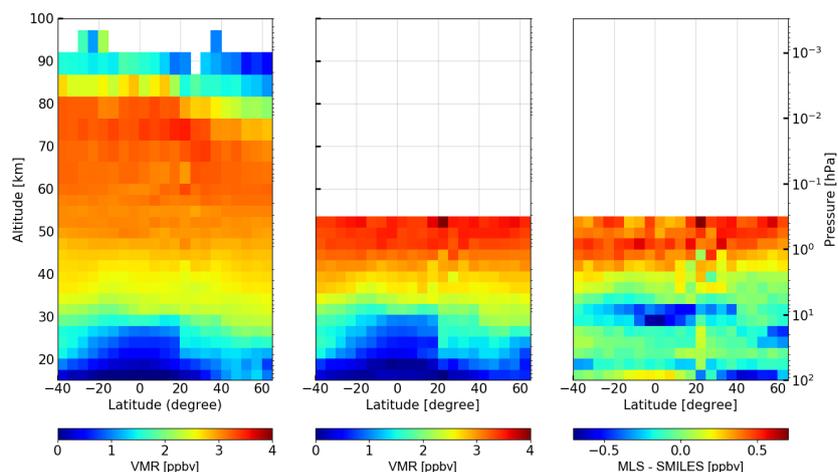
**Figure 6.** Left: SMILES zonal mean HCl profiles versus latitude. Profiles that satisfied coincidence criteria between SMILES and MLS for January 24 – 27, 2010 were used here. Middle: Zonal mean HCl profiles from MLS. Right: The absolute difference of the matched pairs versus latitude.

calibration using a quadratic term for each frequency segment. The details on the TELIS 1.8 THz channel and its L1 data
190  processing are shown in Suttiwong (2010). In this study, we compared two H$^{37}$Cl profiles obtained by TELIS (observation number 20044 and 21537) with the SMILES profiles (Band-B and identifiers 761 and 762) in terms of geolocation and time on January 24, 2010 over Kiruna. The total error of the H$^{37}$Cl profile derived from the TELIS measurement was estimated to be 0.25–0.5 ppbv, with a vertical resolution of 3 km (Xu et al., 2018).

Figure 10 shows a comparison of the HCl vertical profiles of SMILES and TELIS. The left, middle and right panels show the
195  SMILES and TELIS HCl vertical profiles, their absolute difference, and their relative difference, respectively. We converted the H$^{37}$Cl amount to HCl using the natural isotopic abundance (H$^{37}$Cl/HCl = 0.2424). The SMILES and TELIS HCl profiles agreed well, within 0.5 ppbv from 17 km to 34 km. A depletion in the HCl profile was observed below 25 km in both the SMILES and TELIS observations. This result is considered to have been caused by chlorine activation in the polar vortex (Webster et al., 1993). Both the SMILES and TELIS profiles agree well in general, but the TELIS profiles are larger than the
200  SMILES profiles above 32 km (8 hPa). The H$^{37}$Cl line is still rather strong at higher altitudes, and the dominant error source of the TELIS data stems from the non-linearity in the calibration process, which shows that even a small uncertainty may result in significant errors in the retrieval.
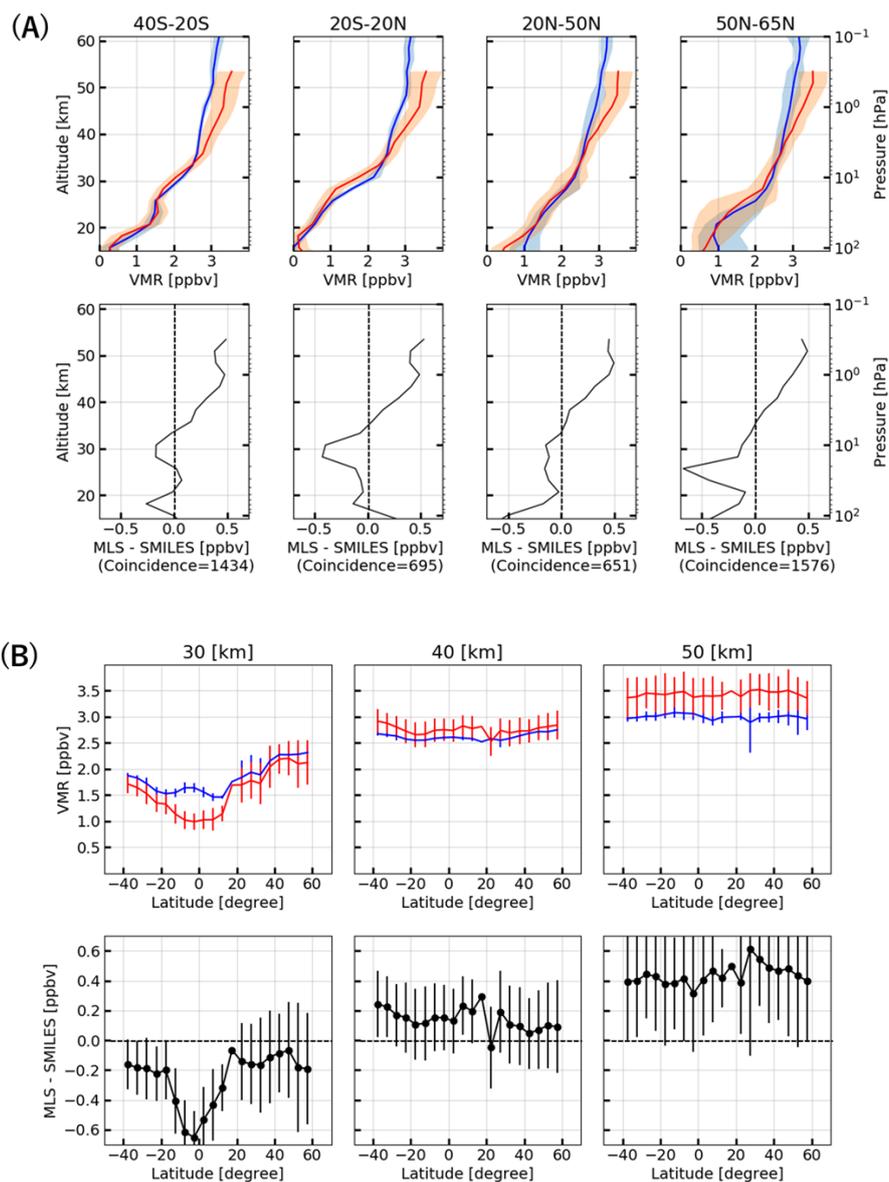
**Figure 7.** (A):Mean HCl profiles, 1 $\sigma$ uncertainty based on variability (shaded region) and the absolute differences for each latitude region. Upper row: The blue and red lines indicate the mean profiles from SMILES and MLS for 40°S-20°S, 20°S-20°N, 20°N-50°N, and 50°N-65°N (left to right panels). Lower row: The absolute difference between the SMILES and MLS profiles calculated using Eq (4) for each latitude region. (B): Latitudinal variation of SMILES and Aura/MLS HCl profiles at three altitude levels. The profiles were averaged for each 5° bin. Upper row: Mean of SMILES (blue) and MLS (red) profiles for each altitude level. The error bars indicate 1 $\sigma$ uncertainties. Lower row: The means and 1 $\sigma$ of the absolute differences are displayed.
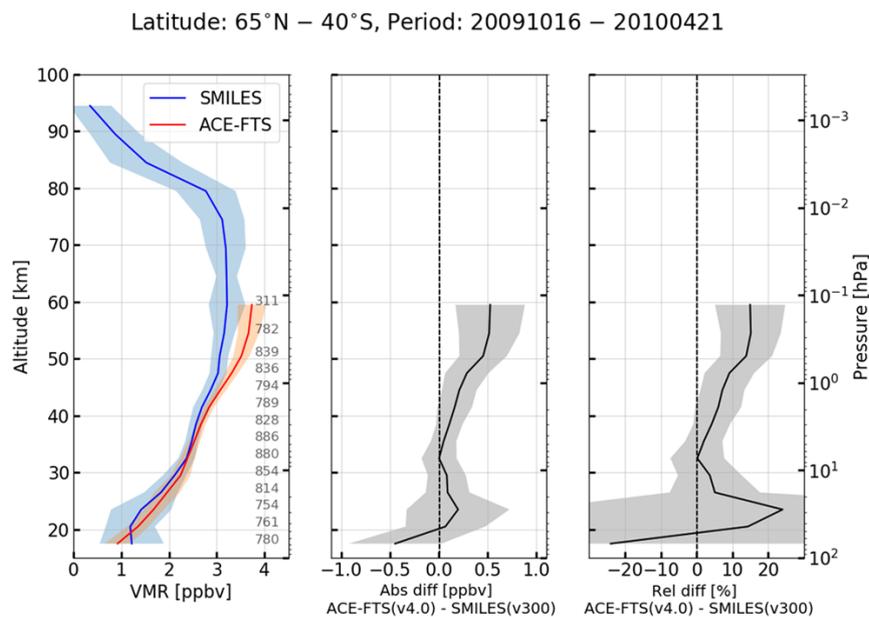
**Figure 8.** Comparison between SMILES and ACE-FTS profiles from October 16, 2009 to April 17, 2010. Left: The mean HCl VMR values (solid lines) and 1 σ (shaded areas) for SMILES and ACE-FTS. The blue and red lines are the SMILES and ACE-FTS HCl profiles, respectively. Middle: The absolute difference between the SMILES and ACE-FTS profiles calculated using Eq (3). Right: The relative difference between the SMILES and ACE-FTS profiles calculated using Eq (4).
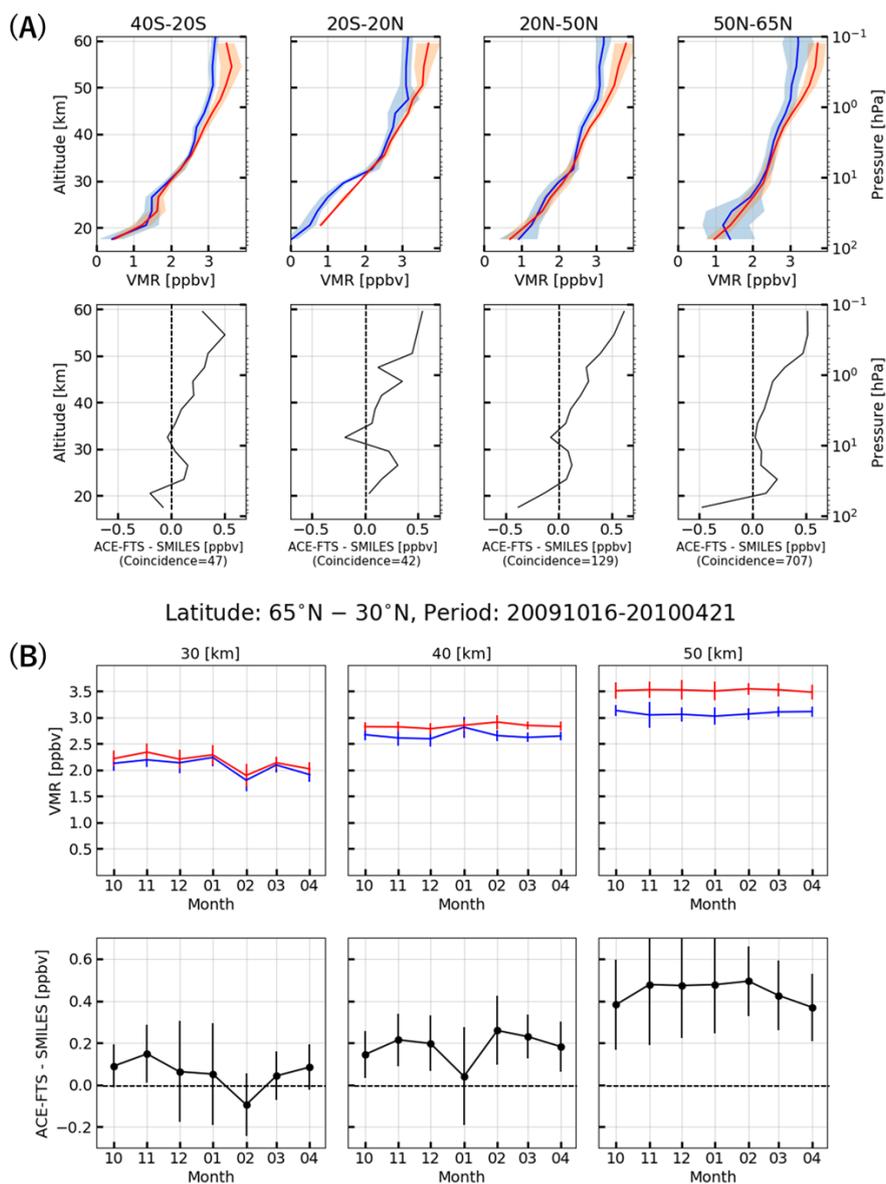
**Figure 9.** Figure-(A): The mean of HCl values, 1 $\sigma$ and the absolute difference for each latitudinal region are shown. Upper row: The blue and red lines indicate the SMILES HCl profiles and ACE-FTS profiles for each latitudinal region, 40°S-20°S, 20°S-20°N, 20°N-50°N, and 50°N-65°N from the left side. Lower row: The absolute difference between the SMILES and ACE-FTS profiles calculated using Eq (3) for each latitudinal region. Figure-(B): Seasonal variation in the SMILES and ACE-FTS HCl profiles at three altitude levels. Latitudinal range is 30°N – 65°N. Upper row: Monthly mean of SMILES (blue) and ACE-FTS (red) HCl profiles for each altitude level. The error bars correspond the 1 $\sigma$. Lower row: The mean and 1 $\sigma$ uncertainty of the absolute difference.
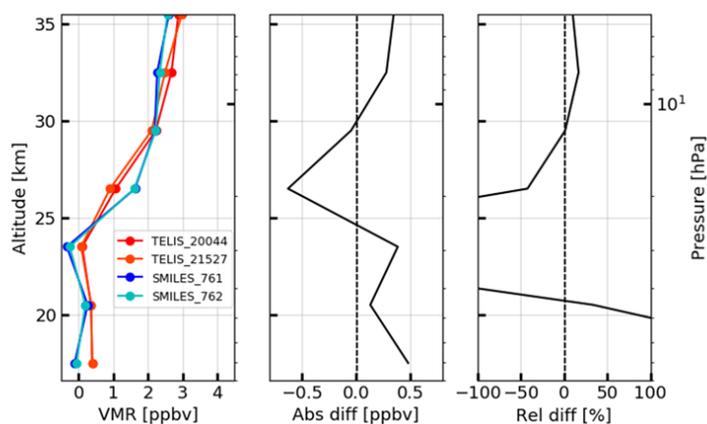
**Figure 10.** Differences between SMILES and TELIS HCl observations are shown for January 24, 2010. Two of the SMILES observations were taken from closer points, where the latitude, longitude, and SZA were 64.3°N, 30.6°E, and 84.6° SZA and 64.8°N, 38.2°E, 86.2° SZA, respectively. Left: Each profile obtained by SMILES and TELIS instruments. Middle: The absolute difference between the SMILES and TELIS profiles calculated using Eq (3). Right: The relative difference between the SMILES and TELIS profiles calculated using Eq (4).

**Table 4.** Summary of the HCl comparison study between SMILES and the other instruments

| Altitude [km] | $\Delta x_{\mathrm{MLS}}$ [ppbv] | $\Delta x_{\mathrm{ACE-FTS}}$ [ppbv] | $\Delta x_{\mathrm{TELIS}}$ [ppbv] |
|:---:|:---:|:---:|:---:|
| 60 | — | 0.5 | — |
| 50 | 0.4 | 0.4 | — |
| 40 | 0.2 | 0.15 | — |
| 30 | -0.2 | 0.05 | $0.4^a$ |
| 20 | -0.1 | -0.02 | $0.5^a$ |

a:The difference between SMILES and TELIS was very large because the coincidence number was only 4.

## 5   Theoretical error analysis

We have evaluated the total error in the HCl vertical profiles observed by SMILES, and we discussed the cause of the bias
205  observed in the comparison study, see Sect. 4.

### 5.1   Estimation of total error

We employed a perturbation method to estimate the total error of the SMILES HCl profile. The details of the perturbation method of the SMILES error analysis have been described in Kasai et al. (2006) and Sato et al. (2014), Kasai et al. (2013), and Sato et al. (2012) for ozone isotopes, ozone, and ClO, respectively. We assumed an averaged HCl profile within the
210  coincidence with MLS in the south mid-latitude region ($20°\mathrm{S} - 40°\mathrm{S}$) as a reference. The total error ($\mathbf{E}_{\mathrm{total}}$) for each altitude grid was calculated by

$$\mathbf{E}_{\mathrm{total}}[\mathrm{i}] = \sqrt{\mathbf{E}_{\mathrm{noise}}[\mathrm{i}]^2 + \mathbf{E}_{\mathrm{smooth}}[\mathrm{i}]^2 + \mathbf{E}_{\mathrm{param}}[\mathrm{i}]^2}, \tag{5}$$

where $\mathbf{E}_{\mathrm{noise}}$ is the error due to spectrum noise, $\mathbf{E}_{\mathrm{smooth}}$ is the smoothing error, and $\mathbf{E}_{\mathrm{param}}$ is the model parameter error. $\mathbf{E}_{\mathrm{noise}}$ and $\mathbf{E}_{\mathrm{smooth}}$ were calculated by

215  $$\mathbf{E}_{\mathrm{noise}}[\mathrm{i}] = \sqrt{\mathbf{S}_{\mathrm{noise}}[\mathrm{i}, \mathrm{i}]} \tag{6}$$

$$\mathbf{S}_{\mathrm{noise}} = \mathbf{D}\mathbf{S}_{\epsilon}\mathbf{D}^{\mathbf{T}} \tag{7}$$

and

$$\mathbf{E}_{\mathrm{smooth}}[\mathrm{i}] = \sqrt{\mathbf{S}_{\mathrm{smooth}}[\mathrm{i}, \mathrm{i}]} \tag{8}$$

$$\mathbf{S}_{\mathrm{smooth}} = (\mathbf{U} - \mathbf{A})\mathbf{S}_{\mathrm{a}}(\mathbf{U} - \mathbf{A})^{\mathbf{T}} \tag{9}$$

220  where $\mathbf{D}$ is the contribution function, and $\mathbf{U}$ is the unit matrix.

We calculated the errors due to the uncertainties of the spectroscopic parameters and the instrument functions to calculate $\mathbf{E}_{\mathrm{param}}$. The error $\mathbf{E}_{\mathrm{param}}$ was calculated by

$$\mathbf{E}_{\mathrm{param}} = I(\mathbf{y}_{\mathrm{ref}}, \mathbf{b}_0 + \Delta \mathbf{b}_0) - I(\mathbf{y}_{\mathrm{ref}}, \mathbf{b}_0) \qquad (10)$$

where $I$ is the inversion function and $\mathbf{b}_0$ is the vector of model parameters. The $\mathbf{y}_{\mathrm{ref}}$ is the reference spectrum calculated using

225    the reference profile. The details of the estimation of the total error are described in Sato et al. (2012). The error sources and perturbations for the model parameter used in this study are summarized in Table 5. These parameters and perturbation value are based on Sato et al. (2014). The uncertainties of the spectroscopic parameters of the $O_3$ transition 625.37 GHz were included to estimate the error due to the interference from the line shape of $O_3$ spectrum. The calibration error was not considered in this study because the latest L1b data version 008 was used and Sato et al. (2014) reported that the error due to the spectrum

230    calibration in this L1b data was insignificant.

**Table 5.** Error sources and their perturbation values for this study.

| Error source | Uncertainty |
| --- | --- |
| Spectroscopic parameters of the $H^{35}Cl$ transition at 625.92 GHz | |
| Line intensity | 1 % |
| Air-pressure broadening coefficient ($\gamma_{\mathrm{air}}$) | 3 % |
| Temperature dependence of $\gamma_{\mathrm{air}}$ ($n_{\mathrm{air}}$) | 10 % |
| Spectroscopic parameters of the $O_3$ transition at 625.37 GHz | |
| $\gamma_{\mathrm{air}}$ of the $O_3$ transition ($\gamma_{\mathrm{air}}$ ($O_3$)) | 3 % |
| $n_{\mathrm{air}}$ of the $O_3$ transition ($n_{\mathrm{air}}$ ($O_3$)) | 10 % |
| Instruments | |
| Antenna beam pattern (Antenna) | 2 % |
| AOS response function (AOS) | 5 % |

The perturbation value was based on Sato et al. (2014).

The estimated errors in the SMILES HCl v300 product are presented in Fig. 11. The total model parameter error, labeled as "Param", was calculated by a root-sum-square (RSS) of all model parameter errors. The three spectroscopic parameters, line intensity, air-pressure broadening coefficient ($\gamma_{\mathrm{air}}$), and its temperature dependence ($n_{\mathrm{air}}$) were dominant error sources below 30 km. The $\gamma_{\mathrm{air}}$ was a major error source between the altitude region of 30 and 60 km, which was about 0.9 ppbv ($\sim$

235    3%) at 50 km. At altitudes of 60–90 km, the largest error source was the AOS response function, and its peak value reached 0.38 ppbv ($\sim$12%) at 70 km.

**5.2   Discussion: Cause of the negative bias of the SMILES HCl vertical profile**

In Sect. 5.2, we discuss the cause of the negative bias of the SMILES HCl vertical profile, i.e., approximately 10 % less than those of Aura/MLS and ACE-FTS especially at the altitudes above 40 km. Such a large bias could not be explained by the total
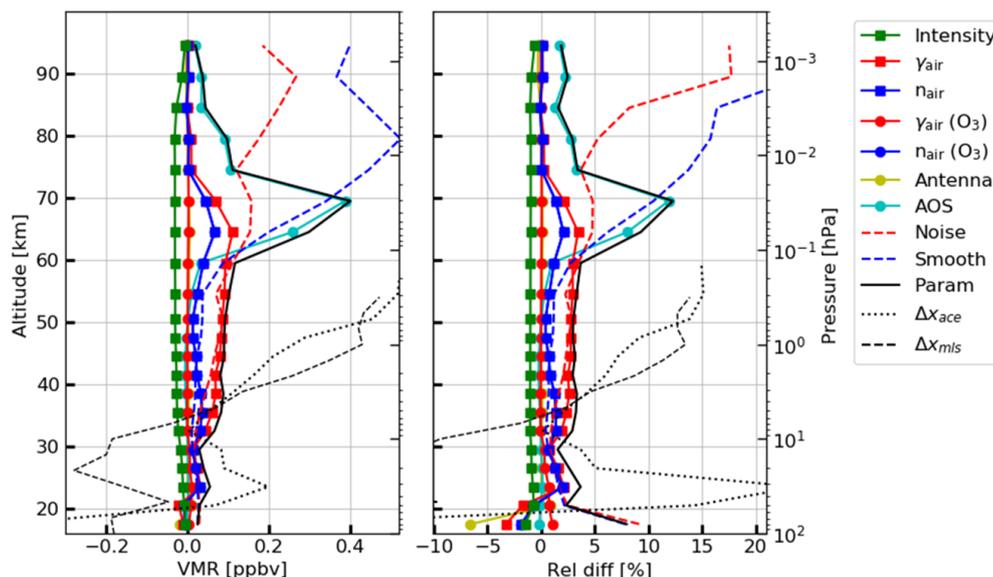
**Figure 11.** Summary of the errors for a single scan observation. The left and right panels, respectively, show the absolute difference and relative difference, which were estimated using the perturbation method. The green marker indicates an error due to the uncertainty in line intensity ("Intensity"). The red and blue square show errors for the air broadening coefficient ("$\gamma_{air}$"), and its temperature dependence ($n_{air}$) of the H$^{35}$Cl transition. The red and blue circles show errors for "$\gamma_{air}$" and $n_{air}$ of the O$_3$ transition ("$\gamma_{air}$ (O$_3$)", "$n_{air}$ (O$_3$)"). The yellow and cyan symbols show errors for the antenna beam pattern ("Antenna"), and the AOS response function ("AOS"). The red and blue dashed lines indicate $\mathbf{E}_{noise}$ ("Noise") and $\mathbf{E}_{smooth}$ ("Smooth"), respectively. The black solid lines ("Param") indicate the total model parameter errors, obtained from the RSS of all the estimated parameter errors. The black dotted and dashed lines indicate the difference between SMILES and MLS, and between SMILES and ACE-FTS.

240   error estimated by the perturbation method described in Sect. 5.1. We further investigated the cause of this bias by difference of temperature profile used in the retrieval calculation. The temperature profile used for the retrieval procedure of SMILES was smaller than those of MLS and ACE-FTS particularly in the upper stratosphere, mesosphere, and lower thermosphere. We estimated the difference of the retrieved HCl vertical profile, $\Delta x$, due to the difference of the temperature profile, $\Delta T$, as follows.

245   $$\Delta x = \mathrm{D} \mathrm{K}_T \Delta T, \quad \mathrm{D} = \frac{\partial x}{\partial y}, \quad \mathrm{K}_T = \frac{\partial y}{\partial T} \tag{11}$$

The jacobian $\mathrm{K}_T$ indicates the sensitivity of the spectral brightness temperature ($y$) with reference to changes of the temperature ($T$). Here we synthesized the jacobian with perturbation of 0.5 K. Figure 12 (A) shows the jacobian as a function of the tangent height. Here the minimum value of the column of the $\mathrm{K}_T$ matrix is plotted. Negative value of the jacobian means that higher temperature synthesizes lower smaller brightness temperature spectrum, thus, increases the HCl abundance in the retrieval

250 calculation to compensate for the underestimation of the synthesized spectrum due to the temperature higher than the true value.

The vertical profile of temperature used for the retrieval procedure of SMILES, MLS, and ACE-FTS and their differences, MLS−SMILES, ACE-FTS−SMILES, are shown in the panels (B) and (C) in Fig. 12, respectively. The vertical profile of temperature of SMILES is approximately 5-10 K smaller than those of both MLS and ACE-FTS at the altitude 50–70km. The

255 panel (D) shows the $\Delta x$ due to the difference of the temperature profile. The difference of the temperature profile caused increase HCl abundance by 0.12 and 0.20 ppbv at about 55 km for MLS and ACE-FTS, respectively.

In the comparison study, see Sect. 4, we confirmed the negative bias in the SMILES HCl vertical profile of 0.4±0.38 and 0.5±0.28 ppbv at 55 km for MLS and ACE-FTS, respectively. We estimated the total error by the perturbation method and investigated the temperature profile used in the retrieval calculation, in order to investigate the cause of this negative bias. The

260 largest error sources were the uncertainties in $\gamma_{air}$ of the H$^{35}$Cl transition and temperature profile used in retrieval calculation. We assumed the 3 % uncertainty in $\gamma_{air}$ and it might cause approximately 0.1 ppbv negative bias at 55 km. The difference in temperature profiles used in the retrieval between SMILES and ACE-FTS caused approximately 0.2 ppbv negative bias. Totally, 0.3 in 0.5 ppbv (60 %) negative bias between SMILES and ACE-FTS was explained by the uncertainty in $\gamma_{air}$ and temperature profile used in the retrieval. The effect of $\gamma_{air}$ error on the negative bias between SMILES and MLS is less than

265 that of SMILES and ACE-FTS, since the SMILES and MLS observed the same H$^{35}$Cl transition lines and the values of the $\gamma_{air}$ are consistent within approximately 1 % (3.39 MHz/Torr for SMILES and 3.42 MHz/Torr for MLS (Drouin, 2004)). The 1 % difference of $\gamma_{air}$ might cause the HCl abundance increase about 0.03 ppbv at 55 km according to our error analysis with a perturbation method. The 0.15 in 0.4 ppbv (approximately 40 %) negative bias between SMILES and MLS was explained. Conclusively, our theoretical error analysis showed that the SMILES HCl a had negative bias of 0.2–0.25 ppbv at 55 km which

270 were consistent with the difference from the MLS and ACE-FTS within the 1 $\sigma$ standard deviation.

## 6 Conclusion

In this study, the HCl vertical profile in a wide range from the upper troposphere to the lower thermosphere was reported for the first time using the SMILES NICT Level 2 data product v300. The HCl vertical profile showed an increase with the altitude increased below the stratopause (∼45 km), approximately constant between the stratopause and the upper mesosphere

275 (∼80 km), and decreased with the altitude increased from the mesopause to the lower thermosphere (∼100 km). This behavior was reproduced by the SD-WACCM model, and the SMILES HCl vertical profile agreed well with the SD-WACCM model within ±0.1 ppbv at altitude 30 to 70 km.

The data quality of the SMILES HCl vertical profile was quantified by the comparison study with other instrument measurements and the theoretical error analysis. We compared the SMILES HCl vertical profiles with well validated data of two

280 satellite instruments, Aura/MLS and ACE-FTS, as well as a balloon-borne instrument, TELIS, at their temporal-spatial coincidence. The SMILES HCl profiles at 20–40 km showed good agreements within less than 0.25±0.3 (1$\sigma$) and 0.20±0.2 (1$\sigma$) ppbv with the MLS and ACE-FTS, respectively. The comparison with the TELIS in polar winter region at 20–34 km
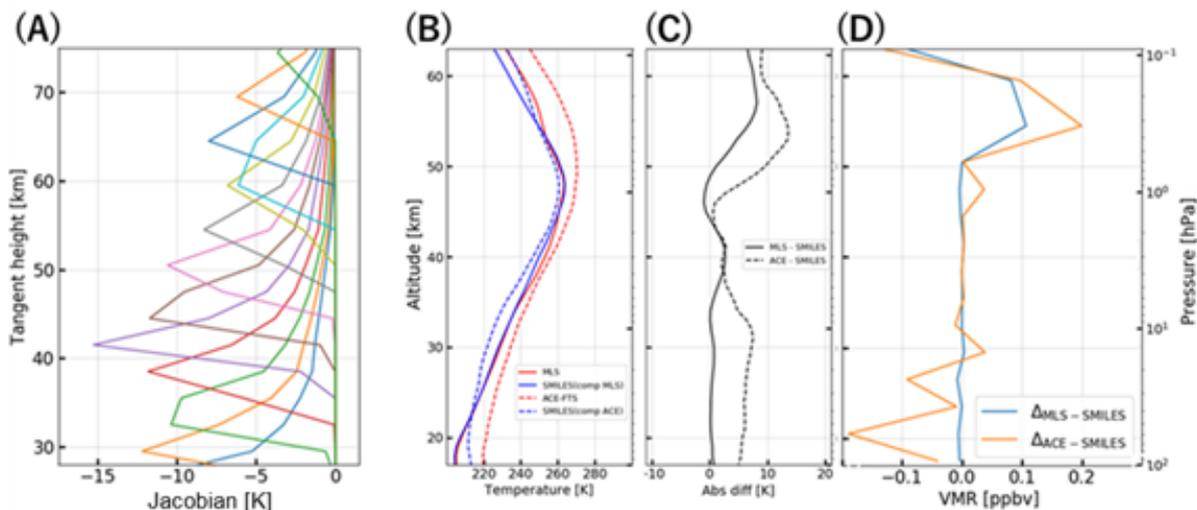
**Figure 12.** (A) The dashed lines represent the jacobian for the temperature calculated using the mean profile from the SMILES winter mid-latitude region (20°S–40°S). The units of the jacobian (x-axis) are Kelvin. (B) Temperature profile of each instruments. The blue and red solid lines indicate the mean SMILES and MLS temperature profiles within the coincidence criteria used for the HCl comparisons. The blue and red dash lines indicate the SMILES and ACE-FTS temperature profiles for the same coincidence criteria. (C) The absolute difference of temperature profiles between SMILES and other instruments calculated using Eq (3 (D) The difference in HCl profiles calculated using Eq (11)

showed similar behavior within the difference of 0.3 ppbv, which is the same order of magnitude as the systematic error of the TELIS data. The negative bias (<0.5 ppbv) of the SMILES HCl profiles from 40 to 60 km altitudes was observed compared to the MLS and ACE-FTS.

We estimated the total error based on the perturbation method and error due to the uncertainty in the atmospheric temperature profile used in the retrieval calculation. The dominant contributions to the systematic errors were from the air broadening parameter (0.09 ppbv) and the AOS response function (0.38 ppbv) at 30–60 km and 60–100 km altitudes, respectively. The uncertainty in the temperature profile used in the retrieval calculation caused the negative bias of 0.12 and 0.20 ppbv at about 55 km, which was 30% and 40% of the HCl abundance difference between SMILES and MLS, and SMILES and ACE-FTS, respectively. The uncertainties of the air broadening parameter and the temperature profile were capable of totally contributing up to 40 – 50% of the negative bias in 50–60 km altitudes. Totally, our theoretical error analysis showed that the SMILES HCl had negative bias of 0.20–0.25 ppbv at 55 km which were consistent with the difference from the MLS and ACE-FTS within the 1 $\sigma$ standard deviation. The spectroscopic parameters of the HCl transitions and the temperature profile above stratosphere are key parameters for further improvement of retrieval algorithm.

The observation of HCl abundances in the upper atmosphere is important to investigate the long-term quantitative estimations of the total budget of anthropogenic chlorine in the Earth's atmosphere. Further observations and model studies regarding

HCl abundance including upper atmosphere are needed to understand the source and sink, transport processes, and chemical reactions related to HCl.

300 *Data availability.* The SMILES data is available at http://smiles.nict.go.jp/pub/data/index.html.

The MLS data is available at https://mls.jpl.nasa.gov/data/.

The ACE-FTS data is available at http://www.ace.uwaterloo.ca/instruments_acefts.php

The details on the TELIS 1.8 THz channel and its L1 data processing are shown in https://elib.suub.uni-bremen.de/edocs/00101711-1.pdf

The WACCM data is available at https://www2.acom.ucar.edu/gcm/waccm

305 *Author contributions.* SN designed the study and performed the analysis. YK designed the study and provided the SMILES data. TOS provided the code for the error analysis and contributed to data analysis and interpretation. TY, TF, and KK contributed to the data analysis and reviewed the manuscript. LF, NJL, KAW, JX, and FS provided MLS, ACE-FTS, and TELIS information and knowledge of HCl in the atmosphere. YJO and VL performed and provided the WACCM simulations. NK and TM supervised writing of and reviewed the manuscript.

*Competing interests.* The authors declare that no competing interests are present.

310 *Acknowledgements.* The JEM/SMILES mission is a joint project of the Japan Aerospace Exploration Agency and the National Institute of Information and Communications Technology. The authors wish to acknowledge the contributions made by their colleagues at JAXA and NICT for managing and supporting the SMILES mission. The authors also thank K. Muranaga (Systems Engineering Consultants Co., Ltd.) and J. Moller (Molflow Co., Ltd.) for supporting the data processing in the SMILES NICT Level2 product. YK is supported by a Funding Program for Next Generation World-Leading Researchers (NEXT Program) (No. GR101).

# References

Baron, P., Urban, J., Sagawa, H., Möller, J., Murtagh, D. P., Mendrok, J., Dupuy, E., Sato, T. O., Ochiai, S., Suzuki, K., Manabe, T., Nishibori, T., Kikuchi, K., Sato, R., Takayanagi, M., Murayama, Y., Shiotani, M., and Kasai, Y.: The Level 2 research product algorithms for the Superconducting Submillimeter-Wave Limb-Emission Sounder (SMILES), Atmospheric Measurement Techniques, 4, 2105–2124, https://doi.org/10.5194/amt-4-2105-2011, https://www.atmos-meas-tech.net/4/2105/2011/, 2011.

Bernath, P. F., McElroy, C. T., Abrams, M. C., Boone, C., Butler, M., Camy-Peyret, C., Carleer, M., Clerbaux, C., Coheur, P., and Colin, R.: Atmospheric chemistry experiment (ACE): mission overview, Geophys. Res. Lett, 32, L15S01, https://doi.org/10.1029/2005GL022386, 2005.

Birk, M., Wagner, G., Lange, G., Lange, A., Ellison, B., Harman, M., Murk, A., Oelhaf, H., Maucher, G., and Sartorius, C.: TELIS: TErahertz and subMMW LImb Sounder – Project summary after first successful flight, pp. 195–200, 2010.

Boone, C., Jones, S., and Bernath, P.: Data usage guide and file format description for ACE-FTS level 2 data version 4.0 ASCII format, Tech. rep., Atmospheric Chemistry Experiment Science Operations Center, https://database.scisat.ca/level2/ace_v4.0/ACE-SOC-0033-ACE-FTS_ascii_data_usage_and_fileformat_for_v4.0.pdf, 2019.

Cazzoli, G. and Puzzarini, C.: Hyperfine structure of the J= 1 ← 0 transition of (HCl)-Cl-35 and (HCl)-Cl-37: improved ground state parameters, Journal of Molecular Spectroscopy, 226, 161–168, https://doi.org/10.1016/j.jms.2004.03.020, 2004.

Drouin, B. J.: Temperature dependent pressure-induced lineshape of the HCl J=1<-0 rotational transition in nitrogen and oxygen, Journal of Quantitative Spectroscopy and Radiative Transfer, 83, 321 – 331, https://doi.org/https://doi.org/10.1016/S0022-4073(02)00360-6, http://www.sciencedirect.com/science/article/pii/S0022407302003606, 2004.

Froidevaux, L., Jiang, Y. B., Lambert, A., N., L. J., Read, W. G., Waters, J. W., Fuller, R. A., Marcy, T. P., Popp, P. J., Gao, R. S., Fahey, D. W., Jucks, K. W., Stachnik, R. A., Toon, G. C., Christensen, L. E., Webster, C. R., Bernath, P. F., Boone, C. D., Harwood, R. S., Walker, K. A., Pumphrey, H. C., Manney, G. L., Schwartz, M. J., Daffer, W. H., Drouin, B. J., Cofield, R. E., Cuddy, D. T., Jarnot, R. F., Knosp, B. W., Perun, V. S., Snyder, V., W., Stek, P. C., Thurstans, R. P., and Wagner, P. A.: Validation of Aura Microwave Limb Sounder HCl measurements, J. Geophys. Res., 113, D15S25, https://doi.org/10.1029/2007JD009025, 2008.

Kasai, Y., Sagawa, H., Kreyling, D., Dupuy, E., Baron, P., Mendrok, J., Suzuki, K., Sato, T. O., Nishibori, T., Mizobuchi, S., Kikuchi, K., Manabe, T., Ozeki, H., Sugita, T., Fujiwara, M., Irimajiri, Y., Walker, K. A., Bernath, P. F., Boone, C., Stiller, G., von Clarmann, T., Orphal, J., Urban, J., Murtagh, D., Llewellyn, E. J., Degenstein, D., Bourassa, A. E., Lloyd, N. D., Froidevaux, L., Birk, M., Wagner, G., Schreier, F., Xu, J., Vogt, P., Trautmann, T., and Yasui, M.: Validation of stratospheric and mesospheric ozone observed by SMILES from International Space Station, Atmospheric Measurement Techniques, 6, 2311–2338, https://doi.org/10.5194/amt-6-2311-2013, https://www.atmos-meas-tech.net/6/2311/2013/, 2013.

Kasai, Y. J., Urban, J., Takahashi, C., Hoshino, S., Takahashi, K., Inatani, J., Shiotani, M., and Masuko, H.: Stratospheric ozone isotope enrichment studied by submillimeter wave heterodyne radiometry: the observation capabilities of SMILES, IEEE Transactions on Geoscience and Remote Sensing, 44, 676–693, https://doi.org/10.1109/TGRS.2005.861754, 2006.

Kikuchi, K.-i., Nishibori, T., Ochiai, S., Ozeki, H., Irimajiri, Y., Kasai, Y., Koike, M., Manabe, T., Mizukoshi, K., Murayama, Y., Nagahama, T., Sano, T., Sato, R., Seta, M., Takahashi, C., Takayanagi, M., Masuko, H., Inatani, J., Suzuki, M., and Shiotani, M.: Overview and early results of the Superconducting Submillimeter-Wave Limb-Emission Sounder (SMILES), J. Geophys. Res., 115, D23306, https://doi.org/10.1029/2010JD014379, 2010.

Kreyling, D., Sagawa, H., Wohltmann, I., Lehmann, R., and Kasai, Y.: SMILES zonal and diurnal variation climatology of stratospheric and mesospheric trace gasses: O3, HCl, HNO3, ClO, BrO, HOCl, HO2, and temperature, Journal of Geophysical Research: Atmospheres, 118, 11,888–11,903, https://doi.org/10.1002/2012JD019420, http://dx.doi.org/10.1002/2012JD019420, 2013.

Lamarque, J.-F., Emmons, L. K., Hess, P. G., Kinnison, D. E., Tilmes, S., Vitt, F., Heald, C. L., Holland, E. A., Lauritzen, P. H., Neu,
355   J., Orlando, J. J., Rasch, P. J., and Tyndall, G. K.: CAM-chem: description and evaluation of interactive atmospheric chemistry in the Community Earth System Model, Geoscientific Model Development, 5, 369–411, https://doi.org/10.5194/gmd-5-369-2012, http://www.geosci-model-dev.net/5/369/2012/, 2012.

Limpasuvan, V., Orsolini, Y. J., Chandran, A., Garcia, R. R., and Smith, A. K.: On the composite response of the MLT to major sudden stratospheric warming events with elevated stratopause, Journal of Geophysical Research: Atmospheres, 121, 4518–4537,
360   https://doi.org/10.1002/2015JD024401, https://agupubs.onlinelibrary.wiley.com/doi/abs/10.1002/2015JD024401, 2016.

Livesey, J. N., Read, W. G., Wagner, P. A., Froidevaux, L., Lambert, A., Manney, G. L., Millán Valle, L. F., Pumphrey, H. C., Santee, M. L., Schwartz, M. J., Wang, S., Fuller, R. A., Jarnot, R. F., Knosp, B. W., Martinez, E., and Lay, R. R.: Version 4.2x Level 2 data quality and description document., Tech. Rep. JPL D-33509, Jet Propulsion Laboratory, http://mls.jpl.nasa.gov/data/datadocs.php, 2018.

Mahieu, E., Duchatelet, P., Demoulin, P., Walker, K. A., Dupuy, E., Froidevaux, L., Randall, C., Catoire, V., Strong, K., Boone, C. D.,
365   Bernath, P. F., Blavier, J.-F., Blumenstock, T., Coffey, M., De Mazière, M., Griffith, D., Hannigan, J., Hase, F., Jones, N., Jucks, K. W., Kagawa, A., Kasai, Y., Mebarki, Y., Mikuteit, S., Nassar, R., Notholt, J., Rinsland, C. P., Robert, C., Schrems, O., Senten, C., Smale, D., Taylor, J., Tétard, C., Toon, G. C., Warneke, T., Wood, S. W., Zander, R., and Servais, C.: Validation of ACE-FTS v2.2 measurements of HCl, HF, CCl$_3$F and CCl$_2$F$_2$ using space-, balloon- and ground-based instrument observations, Atmospheric Chemistry and Physics, 8, 6199–6221, https://doi.org/10.5194/acp-8-6199-2008, http://www.atmos-chem-phys.net/8/6199/2008/, 2008.

370   Ochiai, S., Kikuchi, K., Nishibori, T., Manabe, T., Ozeki, H., Mizobuchi, S., and Irimajiri, Y.: Receiver Performance of the Superconducting Submillimeter-Wave Limb-Emission Sounder (SMILES) on the International Space Station, IEEE Transactions on Geoscience and Remote Sensing, 51, 3791–3802, https://doi.org/10.1109/TGRS.2012.2227758, 2013.

Rienecker, M. M., Suarez, M. J., Gelaro, R., Todling, R., Bacmeister, J., Liu, E., Bosilovich, M. G., Schubert, S. D., Takacs, L., Kim, G.-K., Bloom, S., Chen, J., Collins, D., Conaty, A., da Silva, A., Gu, W., Joiner, J., Koster, R. D., Lucchesi, R., Molod, A., Owens, T., Pawson, S.,
375   Pegion, P., Redder, C. R., Reichle, R., Robertson, F. R., Ruddick, A. G., Sienkiewicz, M., and Woollen, J.: MERRA: NASA's Modern-Era Retrospective Analysis for Research and Applications, Journal of Climate, 24, 3624–3648, https://doi.org/10.1175/JCLI-D-11-00015.1, http://dx.doi.org/10.1175/JCLI-D-11-00015.1, 2011.

Russell, J. M., I, Deaver, L. E., Luo, M., Cicerone, R. J., Park, J. H., Gordley, L. L., Toon, G. C., Gunson, M. R., Traub, W. A., and Johnson, D.: Validation of hydrogen fluoride measurements made by the Halogen Occultation Experiment from the UARS platform, J. Geophys.
380   Res., 101, 10 163–10, 1996.

Sato, T. O., Sagawa, H., Kreyling, D., Manabe, T., Ochiai, S., Kikuchi, K., Baron, P., Mendrok, J., Urban, J., Murtagh, D., Yasui, M., and Kasai, Y.: Strato-mesospheric ClO observations by SMILES: error analysis and diurnal variation, Atmospheric Measurement Techniques, 5, 2809–2825, https://doi.org/10.5194/amt-5-2809-2012, https://www.atmos-meas-tech.net/5/2809/2012/, 2012.

Sato, T. O., Sagawa, H., Yoshida, N., and Kasai, Y.: Vertical profile of $\delta^{18}$OOO from the middle stratosphere to lower meso-
385   sphere from SMILES spectra, Atmospheric Measurement Techniques, 7, 941–958, https://doi.org/10.5194/amt-7-941-2014, https://www.atmos-meas-tech.net/7/941/2014/, 2014.

Sato, T. O., Kuribayashi, K., Yoshida, N., and Kasai, Y.: Diurnal variation of oxygen isotopic enrichment in asymmetric-18 ozone observed by the SMILES from space, Geophysical Research Letters, 44, 6399–6406, https://doi.org/10.1002/2016GL071924, https://agupubs.onlinelibrary.wiley.com/doi/abs/10.1002/2016GL071924, 2017.

390   Sugita, T., Kasai, Y., Terao, Y., Hayashida, S., Manney, G. L., Daffer, W. H., Sagawa, H., Suzuki, M., Shiotani, M., Walker, K. A., Boone, C. D., and Bernath, P. F.: HCl and ClO profiles inside the Antarctic vortex as observed by SMILES in November 2009: comparisons with MLS and ACE-FTS instruments, Atmospheric Measurement Techniques, 6, 3099–3113, https://doi.org/10.5194/amt-6-3099-2013, https://www.atmos-meas-tech.net/6/3099/2013/, 2013.

Suttiwong, N.: Development and characterization of the balloon borne instrument TELIS (TErahertz and submillimeter LImb Sounder): 1.8

395   THz receiver, Ph.D. thesis, University of Bremen, 2010.

Waters, J. W., Froidevaux, L., Harwood, R. S., Jarnot, R. F., Pickett, H. M., Read, W. G., Siegel, P. H., Cofield, R. E., Filipiak, M. J., Flower, D. A., Holden, J. R., Lau, G. K., Livesey, N. J., Manney, G. L., Pumphrey, H. C., Santee, M. L., Wu, D. L., Cuddy, D. T., Lay, R. R., Loo, M. S., Perun, V. S., Schwartz, M. J., Stek, P. C., Thurstans, R. P., Boyles, M. A., Chandra, K. M., Chavez, M. C., Chen, G.-S., Chudasama, B. V., Dodge, R., Fuller, R. A., Girard, M. A., Jiang, J. H., Jiang, Y., Knosp, B. W., Labelle, R. C., Lam, J. C., Lee, A. K., Miller, D.,

400   Oswald, J. E., Patel, N. C., Pukala, D. M., Quintero, O., Scaff, D. M., Vansnyder, W., Tope, M. C., Wagner, P. A., and Walch, M. J.: The Earth Observing System Microwave Limb Sounder (EOS MLS) on the Aura Satellite, IEEE T. Geosci. Remote Sens., 44, 1075–1092, https://doi.org/10.1109/TGRS.2006.873771, 2006.

Webster, C. R., May, R. D., Toohey, D. W., Avallone, L. M., Anderson, J. G., Newman, P., Lait, L., Schoeberl, M. R., Elkins, J. W., and Chan, K. R.: Chlorine Chemistry on Polar Stratospheric Cloud Particles in the Arctic Winter, Science, 261, 1130–1134,

405   https://doi.org/10.1126/science.261.5125.1130, https://science.sciencemag.org/content/261/5125/1130, 1993.

WMO: Ozone Depleting Substances (ODSs) and Related Chemicals (Chapter 1), Scientific Assessment of Ozone Depletion 2010, WMO Global Ozone Research and Monitoring Project, Report No. 52, 2010.

Xu, J., Schreier, F., Wetzel, G., De Lange, A., Birk, M., Trautmann, T., Doicu, A., and Wagner, G.: Performance Assessment of Balloon-Borne Trace Gas Sounding with the Terahertz Channel of TELIS, Remote Sensing, 10, https://doi.org/10.3390/rs10020315, https://www.

410   mdpi.com/2072-4292/10/2/315, 2018.

Yamada, T., Sato, T. O., Adachi, T., Winkler, H., Kuribayashi, K., Larsson, R., Yoshida, N., Takahashi, Y., Sato, M., Chen, A. B., Hsu, R. R., Nakano, Y., Fujinawa, T., Nara, S., Uchiyama, Y., and Kasai, Y.: HO Generation Above Sprite-Producing Thunderstorms Derived from Low-Noise SMILES Observation Spectra, Geophysical Research Letters, 47, e60 090, https://doi.org/10.1029/2019GL085529, https://agupubs.onlinelibrary.wiley.com/doi/abs/10.1029/2019GL085529, e60090 10.1029/2019GL085529, 2020.